HAL
open science

Acoustic sensing of forces driving fast capillary flows

Adrien Bussonnière, Arnaud Antkowiak, Francois Ollivier, Michael Baudoin, Régis Wunenburger

To cite this version:

Adrien Bussonnière, Arnaud Antkowiak, Francois Ollivier, Michael Baudoin, Régis Wunenburger. Acoustic sensing of forces driving fast capillary flows. Physical Review Letters, 2020, 124 (8), 084502, 5 p. 10.1103/PhysRevLett.124.084502 . hal-03321545

HAL Id: hal-03321545

https://hal.science/hal-03321545v1

Submitted on 17 Jan 2023

HAL is a multi-disciplinary open access archive for the deposit and dissemination of scientific research documents, whether they are published or not. The documents may come from teaching and research institutions in France or abroad, or from public or private research centers.

L'archive ouverte pluridisciplinaire **HAL**, est destinée au dépôt et à la diffusion de documents scientifiques de niveau recherche, publiés ou non, émanant des établissements d'enseignement et de recherche français ou étrangers, des laboratoires publics ou privés.

Acoustic sensing of forces driving fast capillary flows

Adrien Bussonnière[1,2], Arnaud Antkowiak[1], François Ollivier[1], Michaël Baudoin[2], and Régis Wunenburger[1]
[1]*Sorbonne Université, CNRS, Institut Jean Le Rond d'Alembert, F-75005 Paris, France*
[2]*Univ. Lille, CNRS, ECLille, ISEN, Univ. Valenciennes, UMR 8520 - IEMN, F-59000 Lille, France*
(Dated: November 26, 2019)

The popping sound of a bursting soap bubble is acquired using microphone arrays and analyzed using spherical harmonics decomposition. Using the theoretical framework of aeroacoustics, we demonstrate that this acoustic emission originates mainly from the capillary stresses exerted by the liquid soap film on the air and that it quantitatively reflects the out-of-equilibrium evolution of the flowing liquid film. This constitutes the proof of concept that the acoustic signature of violent events of physical or biological origin could be used to measure the forces at play during these events.

The analysis of the sound emitted or scattered by fluid flows provides a profusion of quantitative information on their causes and features. For example the velocity of in-vivo flowing blood is routinely deduced from the sound scattered by blood. The vorticity field of unsteady flows such as aerodynamic jets or wakes can be analyzed from the sound they either emit ("aerodynamic sound" [1]) or scatter [2, 3]. The size of gas bubbles can be assessed from the frequency of the sound emitted by their free pulsations [4]. At last, the energy of explosions can be deduced from the N-shaped pressure signal they emit [5]. Fluid momentum variation is also known to result in sound radiation. Its detection could, in principle, enable to determine non intrusively the external forces causing the fluid acceleration in situations where they are largely unknown, such as flows triggered by the rupture, coalescence, atomization or impact of liquid free surfaces, films or elastic membranes, or by propulsive, defensive or preying motions of animals. Such a force remote-sensing technique should be considered as a useful complement to high-speed imaging that gives access only to the shapes of the evolving surfaces.

To determine the external forces at play, their acoustic emission has to be discriminated from those due to volume or vorticity variations. As described by the theory of aeroacoustics [1], fluid volume variations result in a monopolar acoustic radiation pattern, whereas fluid momentum variations result in a dipolar pattern and vorticity variations in a quadrupolar one. Thus, these radiation patterns can be discriminated by using microphone arrays and spherical harmonics decomposition [6]. In this letter, we demonstrate that the forces triggering a rapid hydrodynamic event can be quantitatively assessed from the analysis of their acoustic signature acquired using arrays of sensors. To achieve this aim, we focus on the familiar popping sound of a bursting soap bubble, considered as a paradigm of violent flows driven by surface tension. Using the framework of aeroacoustics, we show that the bubble acoustic emission can be mainly ascribed to the capillary stresses exerted by the liquid soap film on the air and that it quantitatively reflects the out-of-equilibrium evolution of the flowing liquid film. This constitutes the proof of concept that acoustic remote sensing can be used to measure the forces driving fluid flows.

Soap bubbles of 1 mL typical volume are blown up with air using a syringe pump atop a vertical capillary tube, see Fig. 1 a. The liquid soap used is a $0.25\ \mathrm{g \cdot L^{-1}}$ sodium dodecyl sulfate (SDS)-water solution with equilibrium surface tension at ambient temperature $\gamma_0 = (50 \pm 1)\ \mathrm{mN \cdot m^{-1}}$ [7]. Bursting events are either spontaneous or triggered using a hydrophobic needle located $10 - 15$ mm above the tube outlet, visible on top of the pictures of bursting bubble shown in Fig. 1 a. As known since more than a century [8], bubble bursting usually begins with the spontaneous or triggered opening of a hole in the soap film followed by the growth of a circular rim gobbling up the soap film in its path at a typical speed $v_\mathrm{r} \sim 10\ \mathrm{m \cdot s^{-1}}$ up to its complete disappearance, as evidenced by the pictures acquired using a high-speed camera [7] shown in Fig. 1 a. In a first series of experiments, the acoustic emission of the bursting bubble is recorded using three circular acoustic antennae each made of eight microphones [7] sketched in Fig. 1 b. The eight pressure signals recorded by the 44 mm radius antenna during the triggered bursting of a fresh bubble, shown in Fig. 1 c, evidence that the bubble radiates sound during the whole bursting duration. Remarkably, although these signals exhibit the same shape, their sign and amplitude depend on the microphone colatitude θ_m (as defined in Fig. 1 b), the signals recorded above and below the bubble having opposite signs: the bursting bubble behaves as an acoustic dipole with vertical axis. To identify the sources of sound during bubble bursting, we compute from the 24 signals the three pressure fields associated respectively to the monopolar, dipolar and quadrupolar radiations by applying spherical harmonics decomposition and spatial filtering [7]. The corresponding three multipolar contributions to the pressure signal measured by the microphone located on the bubble top are shown in Fig. 1 e. Their comparison confirms that the dipolar radiation actually dominates the monopolar and quadrupolar radiations.

Such a simple acoustic signature can be explained by first describing the bursting process. Before bursting, the air contained in the spherical bubble with radius $R \simeq 6$ mm is pressurized at Laplace overpressure

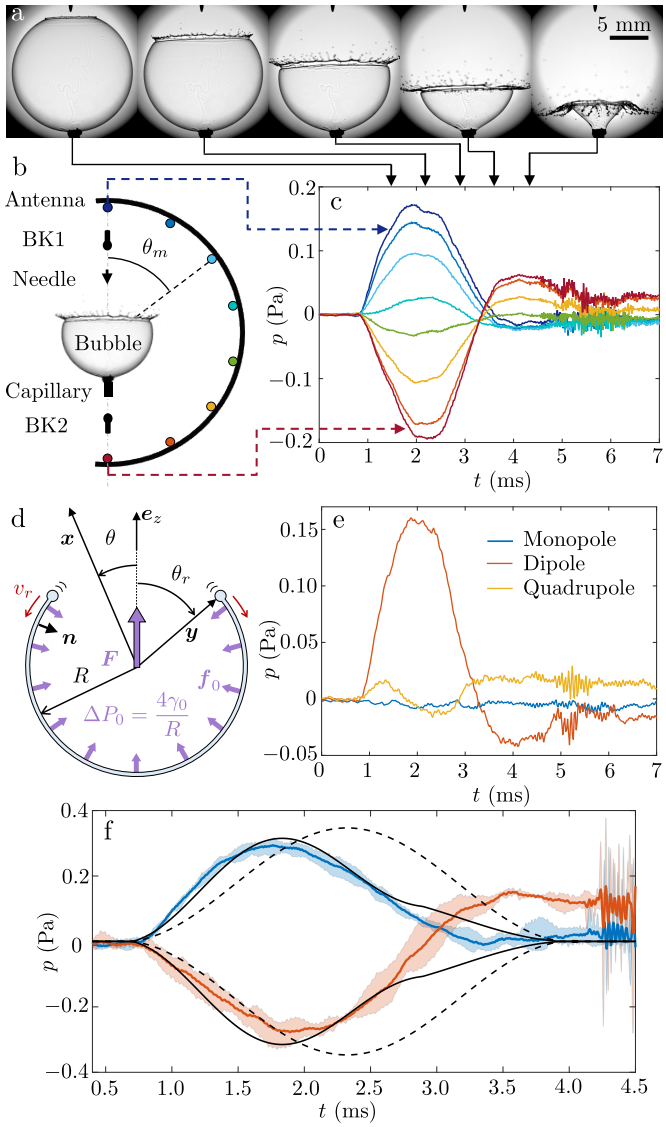

FIG. 1. (a), High speed imaging of the bursting of a 2 mL triggered bubble. (b) Sketch of the setup showing one circular acoustic antennae of eight MEMS microphones (coloured circles) and the two large bandwidth microphones BK1 and BK2. (c) Signals acquired by the 44 mm radius acoustic antenna. (d) Schematic of the bubble bursting showing the capillary forces. (e) Monopolar, dipolar and quadrupolar contributions to the pressure signal measured on the bubble top. (f) Pressure acquired by top BK1 (blue curve) and bottom BK2 (red curve) microphones at 30 mm from a 1 mL fresh bubble. Solid lines correspond to the average over 5 experiments and shaded areas are bounded by the maximum and minimum. Quasistatic model (resp. out-of-equilibrium model) is plotted as dashed lines (resp. solid lines).

$\Delta P_0 = 4\gamma_0/R \simeq 30$ Pa by the isotropic capillary stresses $\mathbf{f}_0 = 2\gamma_0\kappa_0\,\mathbf{n}$ exerted by the two curved liquid-air interfaces constituting the soap film, where $\kappa_0 = 2/R$ is the film curvature and $\mathbf{n}$ the unit vector normal to the film, see Fig. 1 d. According to [9–11], when a hole is formed in the liquid film, the hole rim retracts at the velocity

$$v_\mathrm{r} = \sqrt{\frac{2\gamma_0}{\rho_\mathrm{f} e_0}}, \tag{1}$$

where $\rho_\mathrm{f} = 1.0 \times 10^3$ kg $\cdot$ m^{-3} is the liquid mass density and $e_0 \sim 1$ μm the film typical thickness, as the result of the balance between pulling surface tension and liquid inertia. Thus, film retraction is expected to last for $T = \pi R/v_\mathrm{r} \simeq 5$ ms, in agreement with observations.

As soon as the film opens, the capillary stresses exerted by the soap film on the inner air do not balance anymore, as illustrated in Fig. 1 d. Their addition results in a capillary force $\mathbf{F} = \mathrm{F}\,\mathbf{e}_z$ that varies with the hole opening (see Fig. 1 d). This force accelerates the inner air vertically upward and therefore triggers a dipolar acoustic radiation with vertical axis and duration T. The monopolar radiation due to the expansion of inner air and the quadrupolar radiation due to vorticity production in the rim wake are estimated as negligible compared to the dipolar radiation [7].

During the film opening, the air is accelerated by the capillary stresses $\mathbf{f}(\mathbf{y}, t)$ where $\mathbf{y}$ scans the bursting liquid film at time t (see Fig. 1 d). Linearized Euler equation written for air is thus : $\rho_\mathrm{a}\partial_t\mathbf{v} = -\mathbf{grad}\ p + \mathbf{f}(\mathbf{y}, t)\delta_\mathbf{y}$ where $\mathbf{v}$ is the air velocity, p the acoustic pressure perturbation, ρ_a air mass density at equilibrium, $\delta_\mathbf{y}$ the 1D Dirac function defined along $\mathbf{n}$ and centered on $\mathbf{y}$. Combining it with the linearized equation of mass conservation $\partial_t(c^{-2}p) = -\rho_\mathrm{a}\mathrm{div}\ \mathbf{v}$ (c is the speed of sound in air) results in the linearized equation of propagation $c^{-2}\partial_{tt}p - \Delta p = -\mathrm{div}\ [\mathbf{f}(\mathbf{y}, t)\delta_\mathbf{y}]$. According to [12], the resulting acoustic pressure perturbation p_D at position $\mathbf{x}$ and time t is

$$p_\mathrm{D}(\mathbf{x}, t) = \frac{1}{4\pi} \iint_{\text{film at } t'} \mathrm{div}\left(\frac{\mathbf{f}(\mathbf{y}, t')}{|\mathbf{x} - \mathbf{y}|}\right) \mathrm{d}S \tag{2}$$

where div is the divergence operator with respect to $\mathbf{x}$, $t' = t - \frac{|\mathbf{x}-\mathbf{y}|}{c}$ the retarded time and $\mathrm{d}S$ the elementary film area. For $|\mathbf{x}| \gg R$, Eq. (2) can be approximated by:

$$p_\mathrm{D}(r, \theta, t) = \frac{1}{4\pi r}\cos(\theta)\left[\frac{1}{c}\dot{\mathrm{F}}(t') + \frac{1}{r}\mathrm{F}(t')\right] \tag{3}$$

where $r = |\mathbf{x}|$ and

$$\mathrm{F}(t) = \iint_{\text{film at } t} \mathrm{f}_z(\mathbf{y}, t)\,\mathrm{d}S, \tag{4}$$

is the capillary force exerted by the soap film on the inner air, with $\mathrm{f}_z = \mathbf{f} \cdot \mathbf{e}_z$ and $\dot{\mathrm{F}}$ the time derivative of F [7].

To model the distribution of stresses exerted by the film on the inner air during bursting, we observe that the bubble does not significantly deflate during the rim retraction, as shown in Fig. 1 a. Thus we assume the

liquid film in front of the rim to be at rest and at thermodynamic equilibrium with uniform curvature R and surface tension γ_0 throughout bursting. Accordingly, $\mathbf{f} = \mathbf{f}_0$ along the bursting film and:

$$\mathrm{F}(t) = \Delta P_0 \, \pi R^2 \sin^2 [\theta_\mathrm{r}(t)] \tag{5}$$

where $\theta_\mathrm{r}(t)$ is the rim colatitude defined in Fig. 1 d. In the frame of this quasistatic model, sound emission originates only from film area reduction.

To quantitatively test the validity of this description of sound radiation, in a second series of experiment we use two large bandwidth microphones [7] distant of $r = 30$ mm from a $R = 6.2$ mm bubble and positioned above and below the bubble, named BK1 and BK2 in Fig. 1. The two acoustic pressure signals acquired during the triggered burst of a fresh bubble are compared to their prediction using Eqs. (3), (5) in Fig. 1 f (dashed curve). $\theta_\mathrm{r}(t)$ has been previously extracted from the images of bubble bursting and interpolated at acoustic sampling frequency. The model catches the shape and amplitude of the measured signals but overestimates their duration and maximal amplitude by approximatively 30 % and 10 % respectively. As shown in the following, the limitation of this model does not rely on the description of the acoustic emission process but actually on the roughness of the quasistatic model of film dynamics.

As reported and analyzed in several previous studies [11, 13–15], the opening of a hole in a soap film may put the surfactant monolayers strongly out-of-equilibrium. The decrease of the soap film area resulting from the rim retraction indeed induces a rapid compression of the surfactants located at the film surface. Since their desorption kinetics is generally slow compared to the film shrinking rate, surfactants behave as if they were insoluble [16] and concentrate at the surface. Due to this rapid increase of the surfactant surface concentration, the surface tension of the compressed films decreases and departs from its equilibrium value. Since acoustic emission relies on the unsteadiness of the capillary stresses exerted by the liquid film on the air, the departure of surface tension from its equilibrium value is expected to have a noticeable impact on the acoustic emission during bubble bursting.

To gain insight into the film dynamics, a time-resolved mapping of its thickness distribution during bursting is required. To this aim, long-lived bubbles are considered. Interestingly, due to gravity-driven drainage, such bubbles indeed exhibit strong vertical thickness stratification and film thinning down to thicknesses comparable to visible wavelengths. Consequently, when illuminated by a source of white light and observed in transmission, long-lived bubbles display light interference fringes (see Fig. 2 a) from which the film thickness distribution just before and during bursting can be determined by analyzing the interference patterns [7].

After typically one minute of lifetime, long-lived bubbles ultimately spontaneously burst by opening always at their top where the film is the thinnest. Neglecting the weak departure from sphericity of the bubble during film retraction, the rim velocity $v_\mathrm{r}(t)$ can be calculated from $\theta_\mathrm{r}(t)$ using $v_\mathrm{r} = R\dot{\theta}_\mathrm{r}$. As shown in Fig. 2 b, the variation of $v_\mathrm{r}(\theta_\mathrm{r})$ with the local film thickness before bursting $e_0(\theta_\mathrm{r})$ quantitatively agrees with its prediction using Eq. (1), which demonstrates the validity of Eq. (1) along a curved and stratified soap film.

A careful observation of the light interference pattern during spontaneous bubble bursting events reveals that a thickness discontinuity starting from the hole actually propagates along the film downward ahead of the rim, as indicated by red arrow tips in the pictures shown in Fig. 2 a. The occurence of a thickness shock wave depends on the relation between the out-of-equilibrium surface tension and the surfactant surface concentration that is specific to each surfactant [13]. Shock waves have been observed during film retraction along planar films made of SDS-water solution [11].

Thickness shock wave formation is expected to affect acoustic emission in several aspects. First, the capillary stresses unsteadiness due to the surface tension discontinuity propagating in front of the rim constitutes a supplementary source of sound. Moreover, the shock wave triggers a flow of the soap film that further decreases the stresses exerted by the film on the air, as demonstrated in the following. Assuming a thickness shock wave located at colatitude $\theta_\mathrm{s}(t)$ to propagate at velocity v_s along a planar film initially at rest and at equilibrium, surfactant effective insolubility assumption, mass conservation and momentum balance across the shock indeed entail the motion of the whole film behind the shock wave at velocity $v_\mathrm{f}(\theta_\mathrm{s}^-)$ that satisfies both [13]: $v_\mathrm{f}(\theta_\mathrm{s}^-) = v_\mathrm{s}\,[1 - e_0(\theta_\mathrm{s}^+)/e_1(\theta_\mathrm{s}^-)]$ and $2\,[\gamma_0(\theta_\mathrm{s}^+) - \gamma_1(\theta_\mathrm{s}^-)] = \rho_\mathrm{f}\ e_0(\theta_\mathrm{s}^+)$, where $e_0(\theta_\mathrm{s}^+)$ is the thickness of the film at rest and at equilibrium in front of the shock wave, $e_1(\theta_\mathrm{s}^-)$ and $\gamma_1(\theta_\mathrm{s}^-)$ the thickness of the compressed film and its out-of-equilibrium surface tension behind the shock wave, respectively. Applying these results to a spherical film, behind the shock, each moving fluid element runs a circular trajectory with radius R around the bubble center at tangential velocity v_f (see Fig. 2 c) and is thus subjected to the centripetal acceleration v_f^2/R. Application of second Newton's law to such an accelerated fluid element with thickness e_1 submitted to external pressure P_0, internal pressure P_in and surface tension γ_1, as sketched in the enlargement B in Fig. 2 c, reveals that the centripetal acceleration of the moving film noticeably reduces the overpressure it exerts on the inner air, i.e.

$$\Delta P_1 = P_\mathrm{in} - P_0 = 4\,\frac{\gamma_1}{R} - \rho_\mathrm{f} e_1 \frac{v_\mathrm{f}^2}{R} < 4\frac{\gamma_1}{R}. \tag{6}$$

Such an influence of the tangential film motion on the

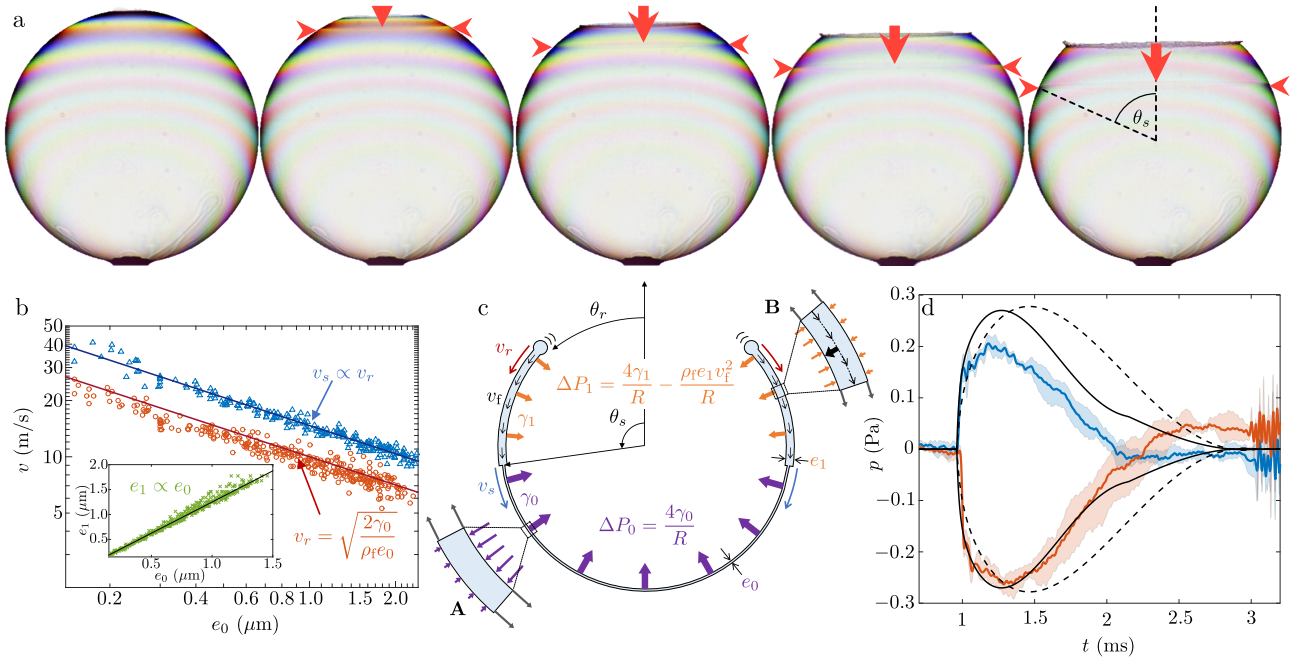

FIG. 2. (a) High-speed images of the spontaneous bursting of a 0.5 mL volume bubble. The red arrow tips indicate the thickness shock wave. (b) Thickness shock wave velocity v_s (blue) and of the rim velocity v_r (red) as function of the initial film thickness e_0. Inset: Film thickness after the shock wave ($e_1(\theta, t)$) versus its initial thickness before the shock wave $e_0(\theta)$. (c) Sketch of the bursting soap bubble illustrating the influence of the shock wave on the bursting dynamic. Enlargements : Capillary forces when the film is at rest (A) and is out-of-equilibrium flowing (B). The in-plane flow induced a centripetal acceleration (bold, black arrow). (d) Pressure signals of the spontaneous bursting of 0.5 mL bubbles recorded by top BK1 (blue curve) and bottom BK2 (red curve) microphones at 30 mm, averaged over three bursting events (solid lines), the shaded areas being bounded by the maximum and minimum of the three signals. Quasistatic model (resp. out-of-equilibrium model) is plotted as dashed lines (resp. solid lines).

pressure jump across curved films is known to be responsible for the large variety of shapes of water bells [17–20].

All the quantities involved in this description of the soap film dynamics can be experimentally assessed from image analysis. As shown in Fig. 2 b, the shock wave velocity inferred from $\theta_s(t)$ using $v_s = R\dot{\theta}_s$ is found to be proportional to v_r, whereas e_1/e_0 is found to be constant along the moving film. These two observations combined with the assumption of surfactant insolubility lead to prove that ΔP_1 is uniform all along the moving film [7]. This leads us to conclude that the only sources of unsteadiness of the capillary stresses, and therefore of acoustic emission, are the moving rim and shock wave. Accordingly, $\mathbf{f} = \Delta P_1\,\mathbf{n}$ in the range $\theta \in [\theta_r(t); \theta_s(t)]$ and $\mathbf{f} = \Delta P_0\,\mathbf{n}$ in the range $\theta \in [\theta_s(t); \pi]$. Use of Eq. (4) results in the following expression for the capillary force exerted by the soap film on the inner air:

$$\mathrm{F}(t) = \pi R^2 \left\{ (\Delta P_0 - \Delta P_1) \sin^2 [\theta_s(t)] + \Delta P_1 \sin^2 [\theta_r(t)] \right\} \tag{7}$$

from which the acoustic emission away from the bubble can be evaluated using Eq. (3) (out-of-equilibrium model).

Fig. 2 d displays typical acoustic signals acquired during the bursting of long-lived bubbles. They are initially steeper than in the case of fresh bubbles, as the consequence of the initially large retraction velocity $v_r \propto e_0^{-1/2}$ of the thin film located on the bubble top combined with the dependence of the radiated sound on $\dot{F} \propto \dot{\theta}_r = v_r/R$. The signals detected by the broadband microphone BK2 located below the bubble are found to be quantitatively described by the out-of-equilibrium model (solid curve). The observed gap between this model and the signal detected by BK1 may be ascribed to a bandwidth narrower than BK2 which affects the high-frequency content of this sharp signal. On the contrary, the agreement between experimental data and the quasistatic model Eqs. (3) and (5) (dashed curve) is only qualitative, as in the case of fresh bubbles.

Extrapolating this refined description of film dynamics to fresh bubbles allows us to predict and to quantitatively describe the propagation of a thickness shock wave along bursting fresh bubbles, although they are made of thick films that display no light interference fringes and hardly visible shock waves. This is possible because the whole description of the film dynamics requires only the knowledge of the equilibrium surface tension γ_0 and of the rim colatitude $\theta_r(t)$ that is as easily measurable on fresh bubbles as on long-lived ones. When applying this refined

model of acoustic emission Eqs (3), (7) to fresh bubbles, we observe a quantitative agreement between the acoustic signals measured during the needle-triggered bursting of fresh bubbles and their prediction (solid curve), as shown in Fig. 1 f. This confirms that the thickness shock wave propagating along the bursting soap film noticeably contributes to sound emission in the case of fresh bubbles too.

We have shown that the description of the acoustic emission by a bursting bubble we propose is fully consistent with the current understanding of soap film retraction dynamics. This demonstrates that the forces at play during the rapid evolution of liquid interfaces and more generally during violent events of physical of biological origin could be determined from remote dipolar acoustic radiation monitoring by spherical harmonics decomposition and integration of Eq. (3), thus potentially constituting a precious diagnostic complementary to high-speed imaging.

[1] M. J. Lighthill, *Waves in Fluids* (Cambridge University Press, 2001).

[2] F. Lund and C. Rojas, Physica D: Nonlinear Phenomena **37**, 508 (1989).

[3] C. Baudet, O. Michel, and W. J. Williams, Physica D: Nonlinear Phenomena **128**, 1 (1999).

[4] M. Minnaert, The London, Edinburgh, and Dublin Philosophical Magazine and Journal of Science **16**, 235 (1933).

[5] G. B. Whitham, *Linear and nonlinear waves* (John Wiley & Sons, 2011).

[6] B. Rafaely, *Fundamentals of spherical array processing* (Springer, 2015).

[7] See Supplemental Material at URL for more details on experimental protocols, data analysis, description of multipolar sound radiation, interference image processing and model of out-of-equilibrium thin film dynamics.

[8] L. Bull, Institut E.-J. Marey (1904).

[9] G. I. Taylor, Proc. R. Soc. Lond. A **253**, 313 (1959).

[10] F. E. C. Culick, J. AppL. Phys. **31**, 1128 (1960).

[11] W. R. McEntee and K. J. Mysels, J. Phys. Chem. **73**, 3018 (1969).

[12] M. S. Howe, *Theory of Vortex Sound* (Cambridge University Press, 2002).

[13] S. Frankel and K. J. Mysels, J. Phys. Chem. **73**, 3028 (1969).

[14] A. Florence and G. Frens, J. Phys. Chem. **76**, 3024 (1972).

[15] P. C. Petit, M. Le Merrer, and A.-L. Biance, J. Fluid Mech. **774** (2015).

[16] B. R. Vijayendran, J. Phys. Chem. **79**, 2501 (1975).

[17] F. Savart, Ann. Chim **54**, 56 (1833).

[18] F. Savart, Ann. Chim. **54**, 113 (1833).

[19] J. Boussinesq, CR Acad. Sci. Paris **69**, 45 (1869).

[20] G. I. Taylor, Proc. R. Soc. Lond. A **253**, 289 (1959).